Chapter 6

Large scale shell model calculations in Ni region : ^{56}Ni as a core

6.1 Introduction

The neutron-rich nuclei near nickel region is one of the fascinating subject because many intensive experimental investigations have been done in last few years [Fra01]. The reason for this interest is two fold. First of all, the evolution of the single-particle structure towards ^{78}Ni constitutes a test ground for the nuclear shell model. Although a doubly magic nature is proposed for this nucleus, it remains poorly understood to which extent the excess of the neutron matter will act upon the nuclear properties. Second motivation is related to the astrophysical r process, which is the mechanism of rapid neutron capture by seed nuclei in explosive stellar environments [Kra93]. While the detailed flow of this reaction network is difficult to establish, it is still supposed to follow a path among the neutron-rich nuclides dictated by the so-called waiting-point nuclei. In particular, it is generally suspected that the ^{78}Ni nucleus plays a privileged role. Therefore, if the predicted magicity around ^{78}Ni weakens or disappears, it may profoundly affect the stellar nucleosynthesis.

Almost all experiments aiming at neutron-rich nickel isotopes have been performed at fragment separator. The first identification of $^{70-74}$Ni and lifetime determination of $^{71-74}$Ni have been carried out through thermal-neutron-induced fission of ^{235}U and ^{239}Pu at the Lohengrin recoil spectrometer of ILL-Grenoble [Ber90]. The fragmentation of ^{86}Kr at the LISE-3 separator of GANIL-Caen has allowed for the investigation of additional microsecond isomers in $^{67-70}$Ni, $^{69,71-72}$Cu [Grz98], and ^{78}Zn [Dau00]. The same reaction at higher beam energies has enabled the mea-

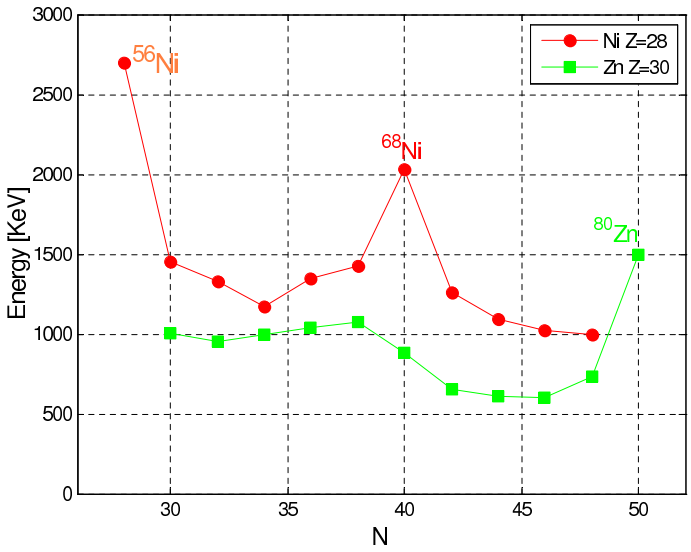

Figure 6.1: Systematic of the experimentally observed E(2_1^+) in the stable and neutron-rich Ni and Zn isotopes near the N=40 and 50 shell closure.

surement of the half-life of $^{73-76}$Ni at the FRS device of GSI-Darmstadt [Ame98]. Attempts to reach exotic nickel and copper by fragmentation of ^{76}Ge have been undertaken at MSU-East Lansing [Huh98, Pri99]. Recently, much effort has been devoted to relativistic fission of the incoming projectile in inverse kinematics. The pioneering work at the FRS machine has been credited with the first identification of ^{77}Ni and long sought ^{78}Ni [Eng95].

The experimental E(2_1^+) for Ni and Zn isotopes are shown in Fig. 6.1. In this figure E(2_1^+) states in Zn are overall lower compared to Ni and an additional decrease of the E(2_1^+) energy in Zn isotopes is obtained between N=40-50 compared to N=28-40. This is probably due to increased π-ν interaction between the two protons outside the Z=28 shell and the N=40-50 neutron shell, which bring in an amount of collectivity.

In the present chapter, large scale shell model calculations have been performed for neutron rich Ni, Cu and Zn isotopes for 40≤N≤50 using code ANTOINE. The low-lying energy levels and BE(2) values have been calculated and compared with the recent experimental data.

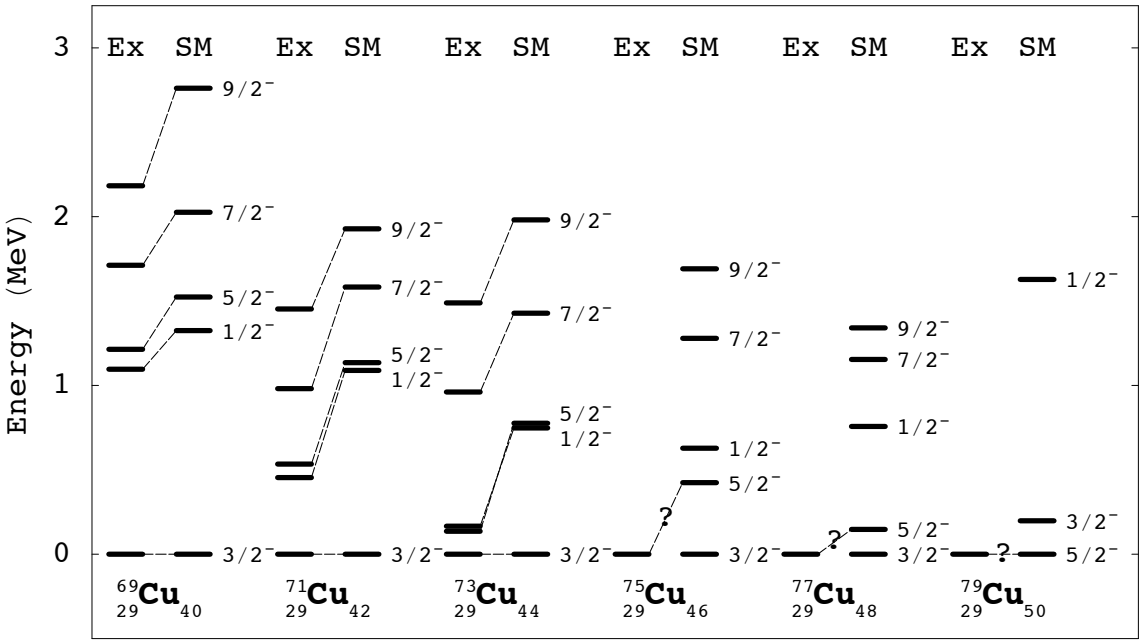

Figure 6.2: Yrast levels of $^{69-79}$Cu isotopes using LSSMI interaction.

6.2 Model space and interaction

The calculations have been performed using $p_{3/2}$, $f_{5/2}$, $p_{1/2}$ and $g_{9/2}$ valence space taking ^{56}Ni as a core. In the present calculation we use two different sets of interactions. The first set of large scale shell model calculations (labeled LSSMI) utilizes the realistic effective nucleon-nucleon interaction based on G-matrix theory by Hjorth-Jensen [Jen95] with the monopole modification by Nowacki [Now96, Smi04]. The second set of calculations (labeled LSSMII) are obtained with the JJ4B effective interaction [Lis04] which is an extension of the renormalized G-matrix interaction based on the Bonn-C *NN* potential (JJ4APN) constructed to reproduce the experimental data for exotic Ni, Cu, Zn, Ge and *N=50* isotones in the vicinity of ^{78}Ni.
The single particle energies for the first set of calculation (LSSMI) for orbital $p_{3/2}$, $f_{5/2}$, $p_{1/2}$ and $g_{9/2}$ are 0.000, 0.770, 1.113 and 3.000 MeV respectively. These single particle energies are taken from experimental data of ^{57}Ni. The single-particle energies for the second set of calculations (LSSMII) for the orbital $p_{3/2}$, $f_{5/2}$, $p_{1/2}$,and $g_{9/2}$ are -9.65660, -9.28590, -8.26950 and -5.89440 MeV respectively.

6.3 Low lying energy levels of $^{69-79}$Cu

The Yrast levels of $^{69-79}$Cu isotopes for ^{56}Ni core using these two interaction are shown in Fig. 6.2-6.3 by indicating Nowacki interaction as (LSSMI) and Lisetskiy interaction as (LSSMII). For $^{69-73}$Cu ground state spin is correctly predicted but other Yrast levels are slightly higher in energy in comparison to the experimental value. For $^{75-77}$Cu, predicted ground state spin is $3/2^-$ whereas the experimental value is $5/2^-$. For ^{79}Cu, predicted spin of $5/2^-$ agrees with the experimental value.

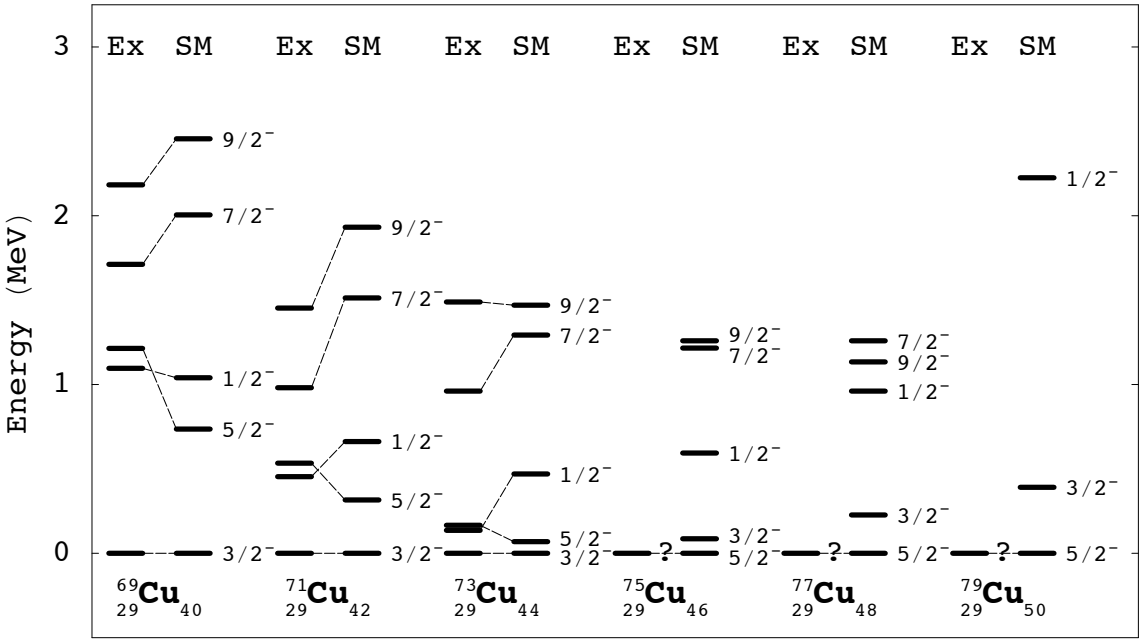

Figure 6.3: Yrast levels of $^{69-79}$Cu isotopes using LSSMII interaction.

The LSSMII calculations predict correct ground state for all the $^{69-79}$Cu isotopes. For ^{69}Cu and ^{71}Cu isotopes Yrast levels are compressed compared to the experimental value. For ^{71}Cu only first $5/2^-$ is lower in energy while the other levels are higher in energy in comparison to the corresponding experimental values. It is observed that in going from ^{69}Cu to ^{79}Cu, as the neutron number increases, the first $5/2^-$ gets lower and lower in energy and becomes the ground state for ^{75}Cu onwards. It is observed that in going from ^{69}Cu to ^{73}Cu energy gap between first excited $5/2^-$ state and $3/2^-$ ground state decreases in energy. For ^{75}Cu the two levels cross each other and $5/2^-$ state becomes the ground state. The gap again rises for ^{79}Cu.

6.4 Low lying energy levels of $^{68-76}$Ni

The low-lying energy levels of $^{68-76}$Ni isotopes are shown in Fig.6.4-6.5 for two interactions. The order of energy levels are well reproduced for both LSSMI and LSSMII interactions. For ^{68}Ni, the first 4^+ state is predicted slightly lower in energy by LSSMI. The LSSMII predicts 2^+ and 4^+ states about at 319 KeV and at 277 KeV above the experimental value. For ^{70}Ni both interactions predict slightly higher energy of the first 2^+ state.

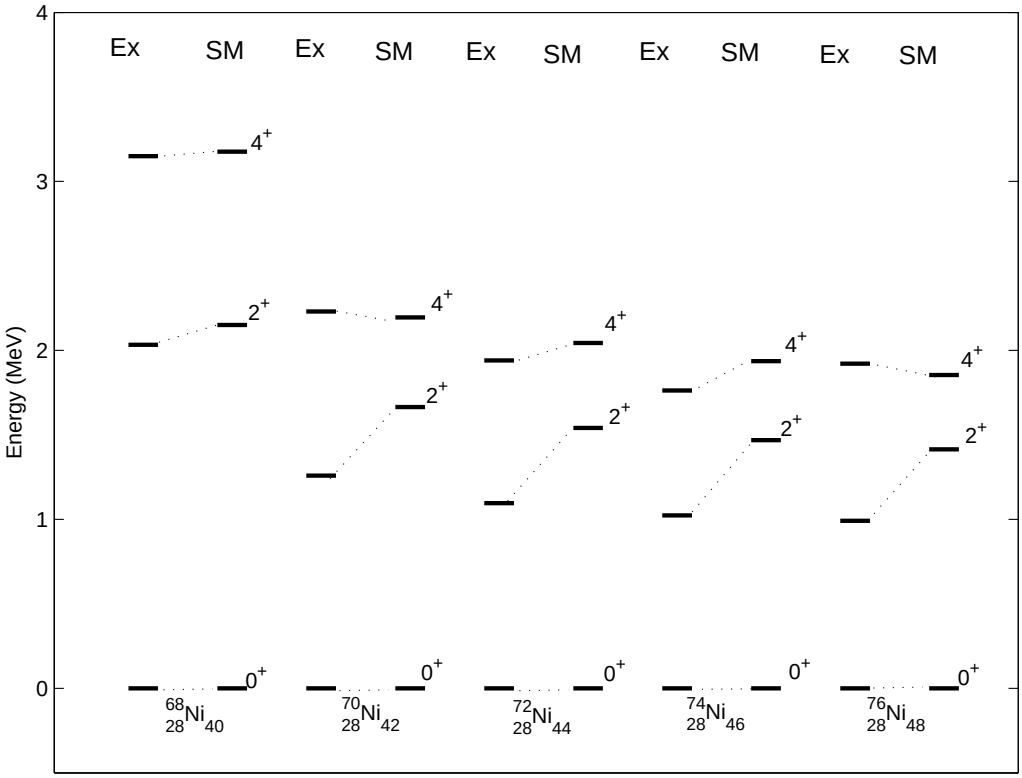

Figure 6.4: Yrast levels of $^{68-76}$Ni isotopes using LSSMI interaction.

LSSMI and LSSMII predict 2^+ state above the experimental value by 406 KeV and 172 KeV. As the number of neutron increases from ^{72}Ni onwards both the interactions predict higher levels nearly 500 KeV higher than the experimental values. Thus both these interaction fail to reproduce the experimental data of more neutron rich Ni isotopes.

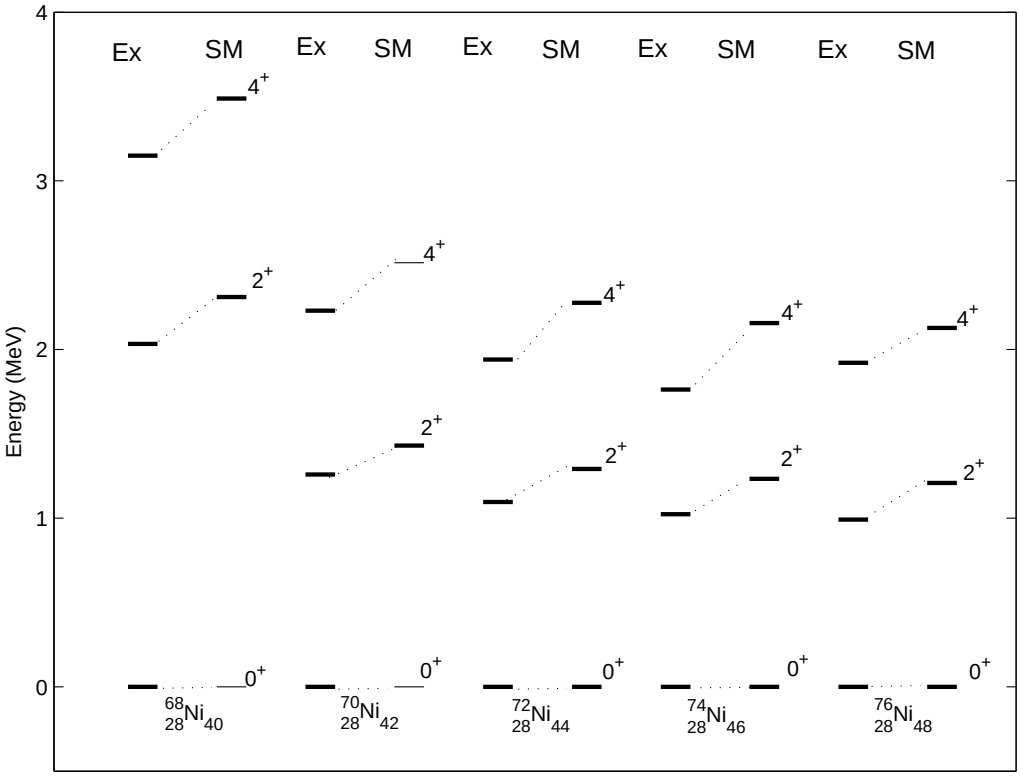

Figure 6.5: Yrast levels of $^{68-76}$Ni isotopes using LSSMII interaction.

The calculated and experimental values of E(2_1^+) and E(4_1^+) for Ni isotopes are shown in Fig. 6.6. The E(4_1^+) energy is well predicted by LSSMI and E(2_1^+) by LSSMII. The high value of E(2_1^+) at N=40 is a clear indication of shell closure.

6.5 Low lying energy levels of $^{70-80}$Zn

The low-lying energy levels of $^{70-80}$Zn isotopes are shown in Fig. 6.7-6.8. For ^{70}Zn both the interactions predict correct order of levels. The first 2^+ state at 885 KeV are predicted at 997 KeV and at 957 KeV by LSSMI and LSSMII interactions respectively. The LSSMII predicts better results for the first 2^+ state. The second 0^+ state is predicted 500 KeV higher than the experimental value. For ^{72}Zn, the order of levels is correctly reproduced by LSSMII. The predicted 2^+ states lie at 302 KeV and at 211 KeV above the experimental value for LSSMI and LSSMII interactions respectively. For ^{74}Zn, 2^+ is predicted at 879 KeV and at 826 KeV by

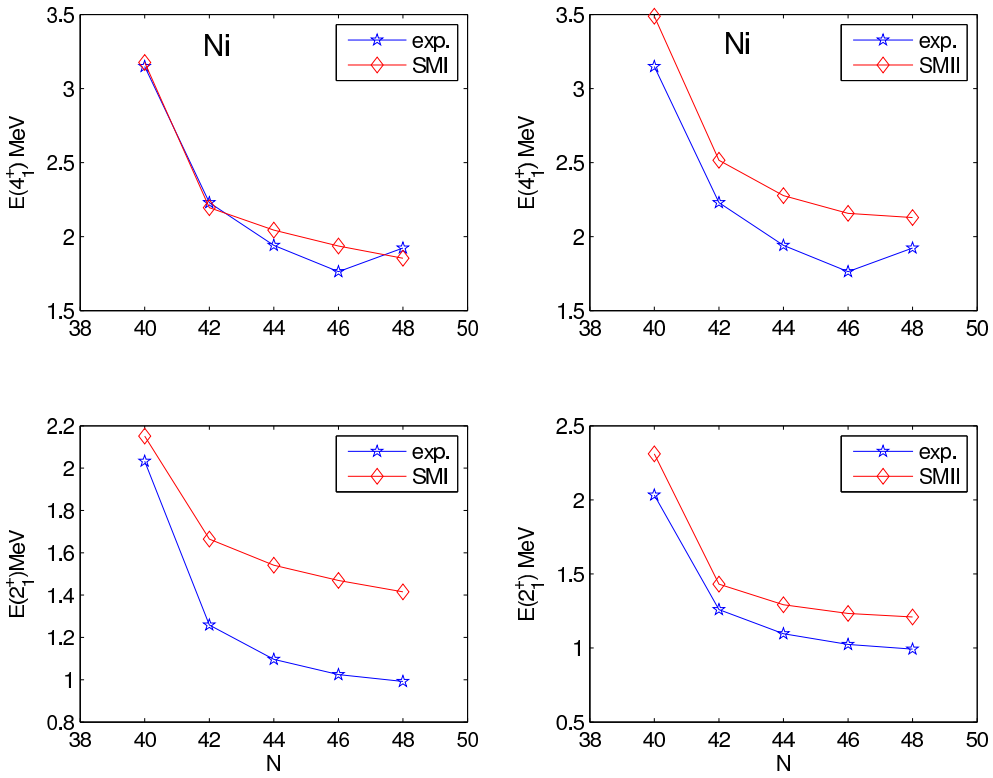

Figure 6.6: The calculated and experimental E(2_1^+) and E(4_1^+) for Ni isotopes as a function of neutron number for LSSMI and LSSMII interactions.

LSSMI and LSSMII whereas the experimental at 606 KeV. The results of LSSMII are better than LSSMI. For ^{76}Zn, the 2^+ at 599 KeV is predicted at 840 KeV and at 911 KeV by LSSMI and LSSMII respectively. The 2^+ in ^{78}Zn at 730 KeV is predicted at 1060 and 1032 KeV and in ^{80}Zn at 1492 KeV is predicted at 1731 KeV and 1353 KeV for LSSMI and LSSMII interactions. Thus as number of neutron increases both these interactions give higher values of 2^+ state in comparison to the corresponding experimental values.

For Zn isotopes, the calculated and experimental values of E(2_1^+) and E(4_1^+) for both the interactions are shown in Fig. 6.9. The E(2_1^+) is predicted correctly by LSSMI interaction. The large value of E(2_1^+) at N=50 is a clear indication of shell closure at N=50.

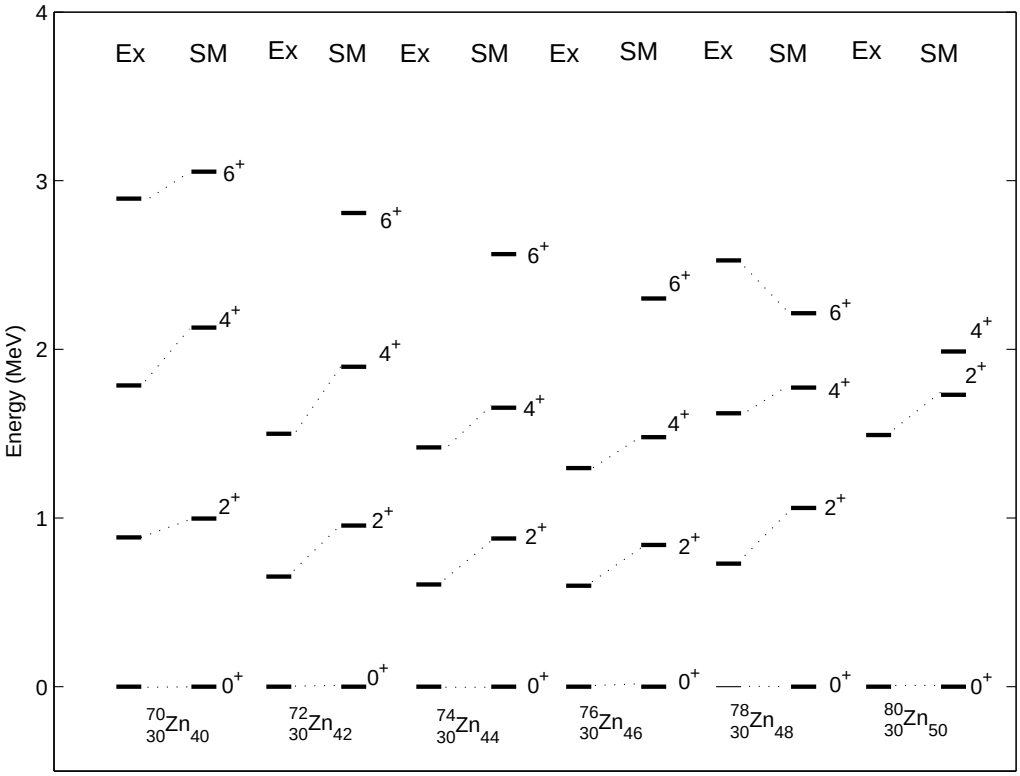

Figure 6.7: Yrast levels of $^{70-80}$Zn isotopes using LSSMI interaction.

6.6 The B(E2) systematics in the Ni isotopes

B(E2; $2_1^+ \rightarrow 0_{gs}^+$) values for Ni isotopes for different set of effective charges for LSSMI and LSSMII are shown in Fig.6.10. The B(E2) for e_π=1.76 and e_ν=0.97 is more closer to experimental values in comparison to the other set of values. The high values of e_π in both LSSMI and LSSMII are required to reproduce experimental results indicating a strong Z=28 core polarization. The high experimental B(E2; $2_1^+ \rightarrow 0_{gs}^+$) in ^{70}Ni is not reproduced for both the interactions. This has been interpreted in Ref. [Per06] as a rapid polarization of the proton core induced by the filling of the neutron $1g_{9/2}$ orbit. This reflects a strong monopole interaction between $\pi 1f_{7/2}$-$\nu 1g_{9/2}$. These results show that the dominance of $g_{9/2}$ orbit in B(E2) calculation is important above N=40.

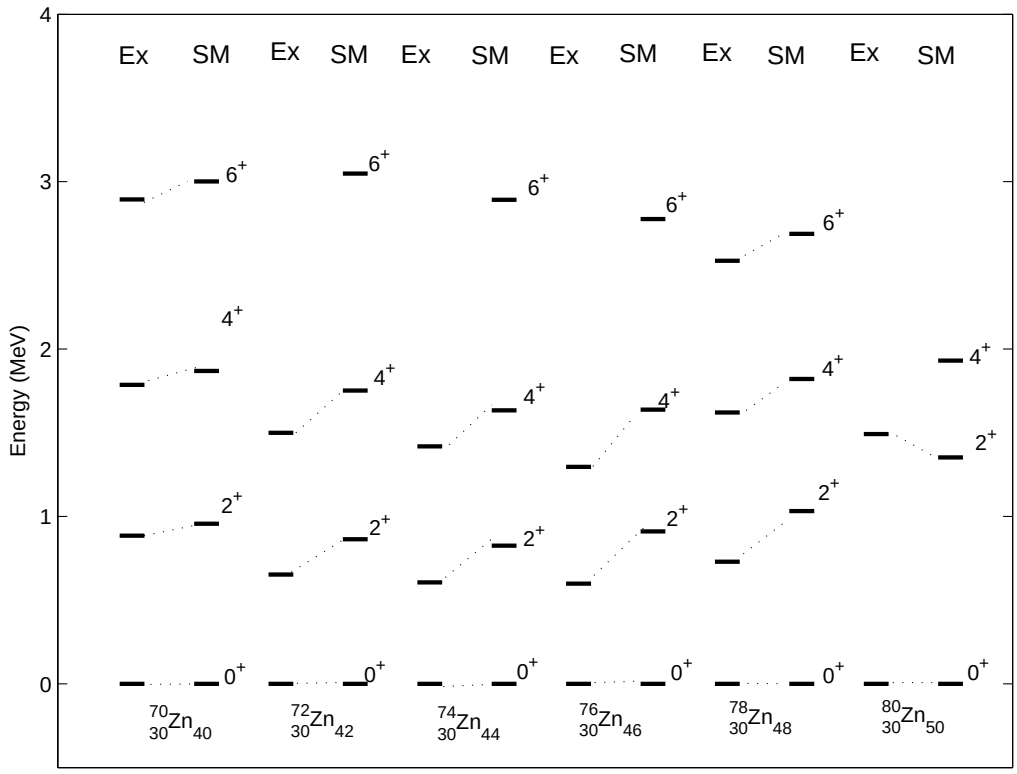

Figure 6.8: Yrast levels of $^{70-80}$Zn isotopes using LSSMII interaction.

6.7 The B(E2) systematics in the Zn isotopes

B(E2; $2_1^+ \rightarrow 0_{gs}^+$) values for Zn isotopes for different set of effective charges for LSSMI and LSSMII are shown in Fig.6.11. This figure show that higher value of e_π is required to reproduce B(E2) correctly. In Zn isotopes above A=68, the contribution from $\nu 1g_{9/2}^2$ configuration in the wave function of the low lying excited 2_1^+ and 4_1^+ states is important. The B(E2;$2_1^+ \rightarrow 0_{gs}^+$) strength is thus dominated by the specific E2 strength between $(\nu 1g_{9/2})_{J=0}$ and $(\nu 1g_{9/2})_{J=0}$ configurations. The increase of the B(E2) values beyond N=40 suggests an incresae of the collectivity induced by the interaction of protons in the *pf* shell and the neutron in $g_{9/2}$ orbit.

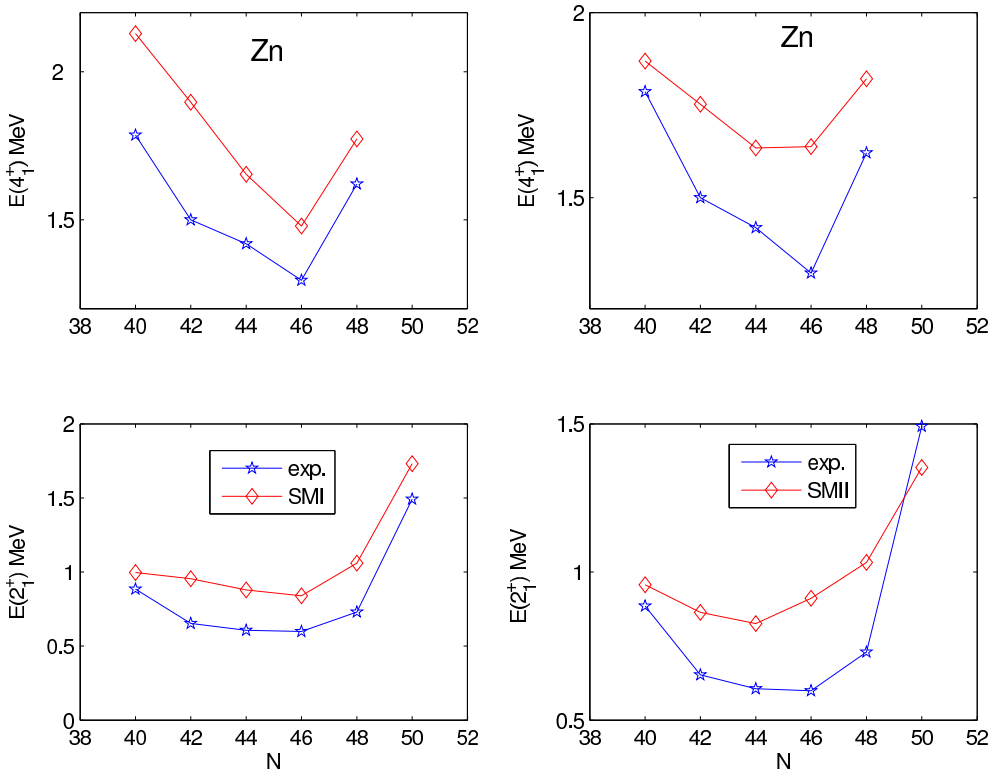

Figure 6.9: The calculated and experimental E(2_1^+) and E(4_1^+) for Zn isotopes as a function of neutron number for LSSMI and LSSMII interactions.

6.8 The occupation numbers

Kaneko *et al.* [Kan08] have shown that the ground-state energies at N=40 show a discontinuity which could correspond to a kind of phase transition at N=40. The occupation number of ground states for Ni and Zn isotopes are shown in Fig.6.12. For the Ni isotopes the occupation of $f_{5/2}$ is higher at N=40. The occupation of $\nu g_{9/2}$ orbital increases and is nearly equal to $p_{1/2}$ at N=42. Further, as neutron number increases, the occupation of $\nu g_{9/2}$ orbital also increases drastically and becomes the most dominant component. For the Zn isotopes, the occupation of $f_{5/2}$ and $p_{3/2}$ is equal at N=40. The occupation of $\nu g_{9/2}$ orbital is same at N=40 and 42 to that of $p_{1/2}$. Beyond that it increases drastically and becomes the dominant component at N=48.

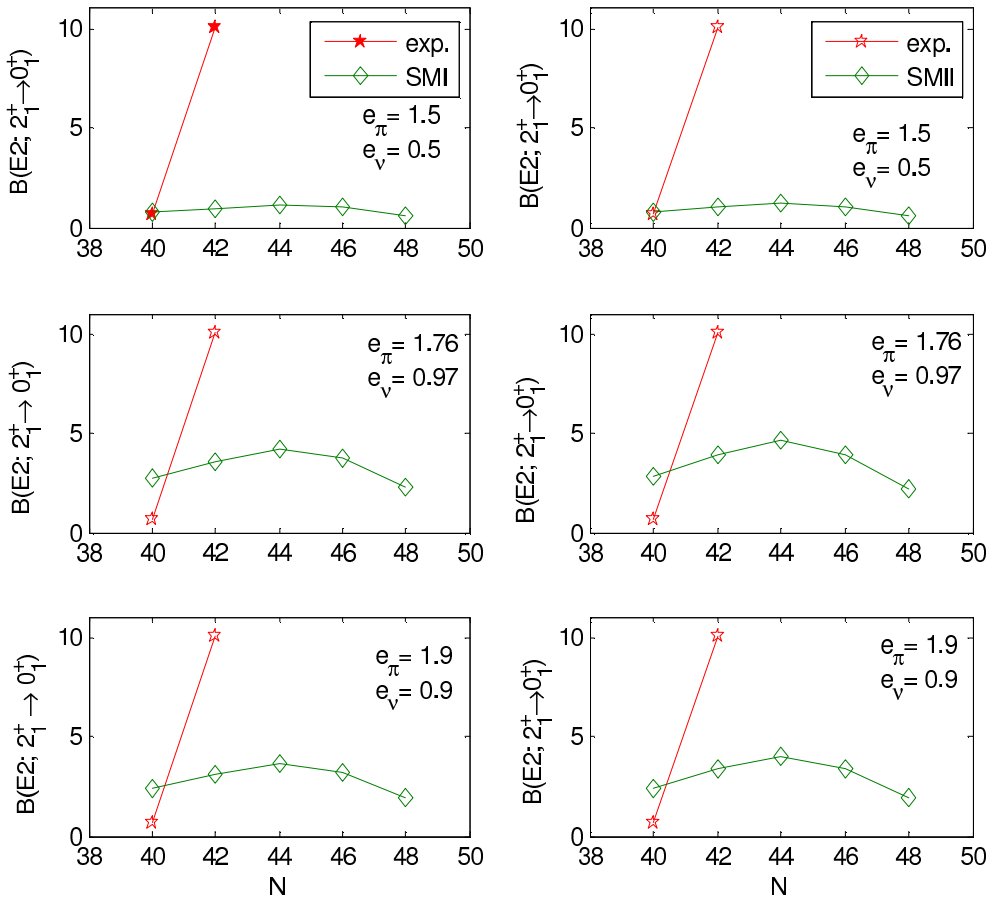

Figure 6.10: The calculated and experimental B(E2;$2_1^+ \rightarrow 0_{gs}^+$) value in W.u. for Ni isotopes as a function of neutron number for LSSMI and LSSMII interactions.

6.9 Conclusions

The large E(2_1^+) values for Ni and Zn isotopes and corresponding low B(E2) values indicate that the inclusion of $f_{7/2}$ orbital is important in model space. The $fpg_{9/2}$ space is suitable for neutron-rich Ni and Zn isotopes beyond N=40. The increase of the B(E2) values beyond N=40 suggests an increase of the collectivity induced by the interaction of protons in the pf shell and neutron in the $g_{9/2}$. In the next chapter, the $fpg_{9/2}$ space have been taken to reproduce these properties for neutron rich Ni, Cu and Zn isotopes beyond N=40.

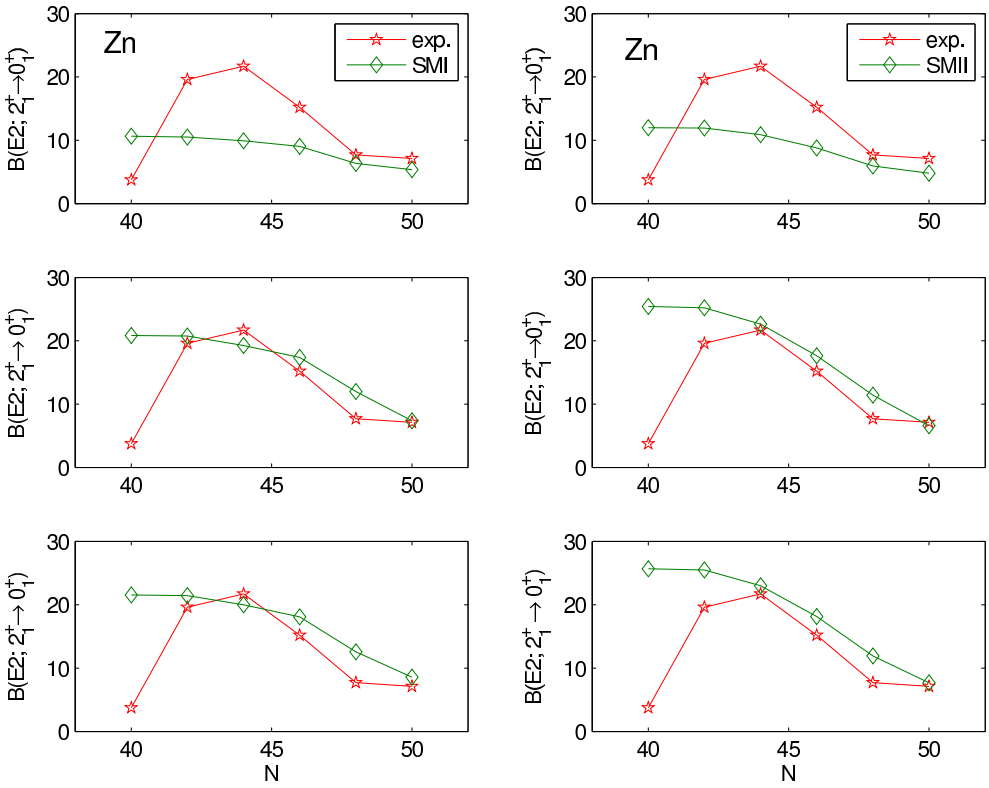

Figure 6.11: The calculated and experimental B(E2;$2^+_1 \rightarrow 0^+_{gs}$) value in W.u. for Zn isotopes as a function of neutron number for LSSMI and LSSMII interactions.

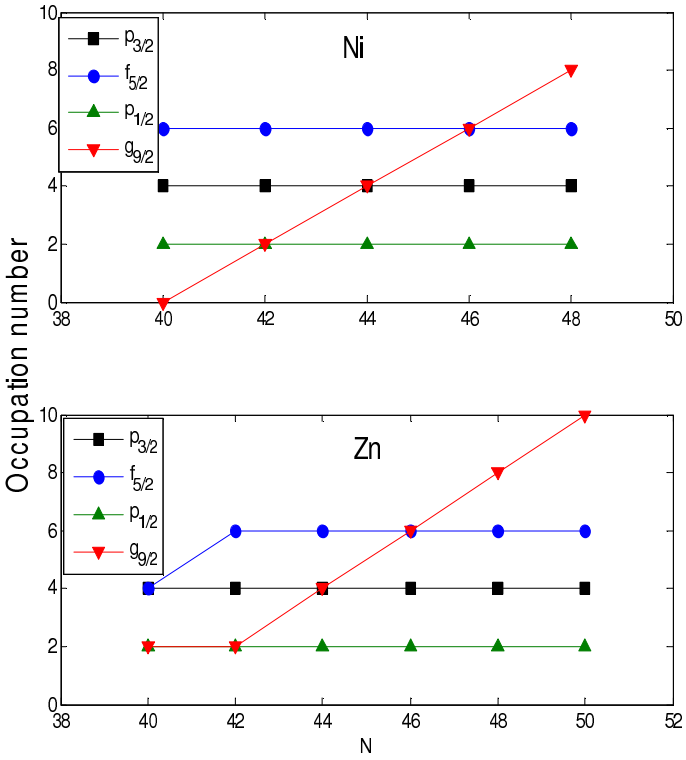

Figure 6.12: Neutron occupation numbers of the Ni and Zn isotopes.